

THERMAL PLASMA IN THE GIANT LOBES OF THE RADIO GALAXY CENTAURUS A

S. P. O'SULLIVAN^{1,2*}, I. J. FEAIN^{1,2}, N. M. MCCLURE-GRIFFITHS¹, R. D. ECKERS¹, E. CARRETTI¹, T. ROBISHAW³,
S. A. MAO^{4,5}, B. M. GAENSLER², J. BLAND-HAWTHORN², L. STAWARZ^{6,7}¹CSIRO Astronomy and Space Science, ATNF, PO Box 76, Epping, NSW 1710, Australia²Sydney Institute for Astronomy, School of Physics, The University of Sydney, NSW 2006, Australia³Herzberg Institute of Astrophysics, Dominion Radio Astrophysical Observatory, PO Box 248, Penticton, BC V2A 6J9, Canada⁴Jansky Fellow, National Radio Astronomy Observatory, P.O. Box O, Socorro, NM 87801, USA⁵Department of Astronomy, University of Wisconsin, Madison, WI 53706, USA⁶Institute of Space and Astronautical Science JAXA, 3-1-1 Yoshinodai, Chuo-ku, Sagami-hara, Kanagawa 252-5210, Japan and⁷Astronomical Observatory, Jagiellonian University, ul. Orla 171, 30-244 Kraków, Poland*Draft version December 11, 2013*

ABSTRACT

We present a Faraday rotation measure (RM) study of the diffuse, polarized, radio emission from the giant lobes of the nearest radio galaxy, Centaurus A. After removal of the smooth Galactic foreground RM component, using an ensemble of background source RMs located outside the giant lobes, we are left with a residual RM signal associated with the giant lobes. We find the most likely origin of this residual RM is from thermal material mixed throughout the relativistic lobe plasma. The alternative possibility of a thin-skin/boundary layer of magnetoionic material swept up by the expansion of the lobes is highly unlikely since it requires, at least, an order of magnitude enhancement of the swept up gas over the expected intragroup density on these scales. Strong depolarisation observed from 2.3 to 0.96 GHz also supports the presence of a significant amount of thermal gas within the lobes; although depolarisation solely due to RM fluctuations in a foreground Faraday screen on scales smaller than the beam cannot be ruled out. Considering the internal Faraday rotation scenario, we find a thermal gas number density of $\sim 10^{-4} \text{ cm}^{-3}$ implying a total gas mass of $\sim 10^{10} M_{\odot}$ within the lobes. The thermal pressure associated with this gas (with temperature $kT \sim 0.5 \text{ keV}$, obtained from recent X-ray results) is approximately equal to the non-thermal pressure, indicating that over the volume of the lobes, there is approximate equipartition between the thermal gas, radio-emitting electrons and magnetic field (and potentially any relativistic protons present).

Subject headings: radio galaxies: individual: Centaurus A (NGC 5128) — radio galaxies: magnetic fields

1. INTRODUCTION

The integrated history of a radio galaxy is encoded in the magnetized, relativistic gas within its lobes. These lobes have been inflated by outflows emanating from the central supermassive black hole (SMBH) of the host galaxy (Begelman et al. 1984) with their structure illuminated by the synchrotron emission we detect in the radio band. Through their formation, radio galaxies can deposit 10^{55} – 10^{62} erg of mechanical energy into the intergalactic medium (IGM) over the lifetime of the source (McNamara et al. 2009), as well as potentially enriching the IGM with heavy elements (Aguirre et al. 2001; Reuland et al. 2007) and magnetic fields (Furlanetto & Loeb 2001). Determining exactly how radio galaxies transfer energy and material to the IGM is essential for understanding their impact on both galaxy and cosmic structure evolution (Bower et al. 2006; Best et al. 2006; Croton et al. 2006). In particular, knowledge of the fraction of “non”-radiating particles (thermal gas and relativistic protons) is of primary importance for understanding the pressure balance and dynamics of radio galaxy lobes with respect to their environments (Morganti et al. 1988; Dunn et al. 2005; Birzan et al. 2008; Croston et al. 2008), as well as their potential to provide seed particles for high energy emission and ultra-high energy cosmic rays (Abdo et al. 2010).

Faraday rotation provides a sensitive diagnostic for the presence of magnetized, ionized thermal material. Previous Faraday rotation studies (Perley et al. 1984; Spangler & Sakurai 1985; Laing & Bridle 1987; Garrington & Conway 1991; Kronberg et al. 2004; Feain et al. 2009) have placed upper limits on the uniform number density of thermal gas within radio galaxy lobes of $\lesssim 10^{-4} \text{ cm}^{-3}$, assuming the minimum-pressure magnetic field intensity. However, conclusively disentangling the different contributions from Faraday rotation that is internal and/or external to radio galaxy lobes has proven very difficult.

In this paper, we present complementary spectropolarimetric observations of the nearest radio galaxy Centaurus A at 1.4 GHz with both the Parkes 64 m single-dish radio telescope and the Australia Telescope Compact Array (ATCA) aperture synthesis telescope. The Parkes observations are sensitive to diffuse emission which allows us to measure the Faraday rotation measure (RM) of the polarized emission from Centaurus A itself, while the high angular resolution ATCA observations (Feain et al. 2009) provide us with an ensemble of RMs from 281 background radio sources that are uncontaminated by any diffuse polarized emission and are located along sightlines both inside and outside the giant lobes. Centaurus A is the only radio galaxy for which such an analysis is possible with current sensitivity due to its large angular size of $\sim 9^{\circ} \times 4^{\circ}$. For a distance to Centaurus A of $\sim 3.8 \text{ Mpc}$ (Harris et al. 2010), 1° corresponds to a

projected linear size of ~ 66 kpc.

In Section 2, we describe the observations, calibration and RM analysis. Section 3 outlines our results along with a discussion on various models and the implication for the giant lobes. Our conclusions are presented in Section 4.

2. OBSERVATIONS AND DATA REDUCTION

2.1. Parkes Data

A $10^\circ \times 14^\circ$ area centred on the position of Centaurus A was observed using the Parkes 64 m telescope at 1.4 GHz over a period of 10 days (2009 March 2–11), totalling 80 hrs of telescope time. The Parkes data used in Feain et al. (2011) were archival but the new observations presented here were required because the archival data did not contain polarisation information. The observations were conducted using a cross-scanning technique with the H-OH receiver and a quarter-wave plate, similar to Mao et al. (2012), providing 0.25 MHz channels across 256 MHz of bandwidth centered on 1388 MHz. The total useable bandwidth covered 1312 to 1480 MHz. The FWHM for the Parkes telescope at 1380 MHz is approximately $14.4'$. Data were obtained while scanning the telescope at a rate of $3^\circ.5 \text{ min}^{-1}$ and sampling every 1 s, meaning that data were recorded every $7'$. This resulted in 120 right ascension (RA) scans and 86 declination (Dec) scans. The data were then imaged with $8' \times 8'$ pixels to ensure at least one data sample per pixel (some blank pixels occurred towards the Northern edge of the image where the scanning rate was slightly too fast for $7' \times 7'$ pixels). This effectively smooths the image and we measure an actual gridded beam width of $\sim 16'$ at 1312 MHz.

Calibration of all scans was done using the Parkes Continuum Polarimetry Software (PARKESPOL)¹ package. The source PKS B1934–638 was used for flux and band-pass calibration due to its bright, stable and well known flux level of 14.95 Jy at 1380 MHz (Reynolds 1994). Basic flagging was done on all scans before the 0.25 MHz channels were rebinned into 8 MHz channels and the polarization calibration was performed on each channel separately. Ten scans of 3C 138 at a range of feed angles from -45° to $+45^\circ$ provided a sufficient range of parallactic angle coverage to calibrate the instrumental polarizations. The polarisation angle calibration was achieved using the known polarization angle of PKS B0043–424 ($+143.3^\circ$ at 1.4 GHz, $\text{RM} = +2 \text{ rad m}^{-2}$, Carretti & Haverkorn, private communication).

Stokes I , Q and U images were created for each frequency channel by combining all RA and Dec scans. Initially, separate RA and Dec maps were created with a linear baseline removal performed using the edge of the image. This removes both the ground emission contamination as well as any structure on scales the size of the map and greater. The final maps are produced by combining the orthogonal scan maps in Fourier space using the technique of Emerson & Graeve (1988) which minimizes the effects of baseline drifts on raster scanned data.

2.2. ATCA Data

Feain et al. (2009) observed an $\sim 45 \text{ deg}^2$ area centred on the host galaxy NGC 5128 with the Australia Tele-

¹ <https://svn.atnf.csiro.au/trac/parkespol>

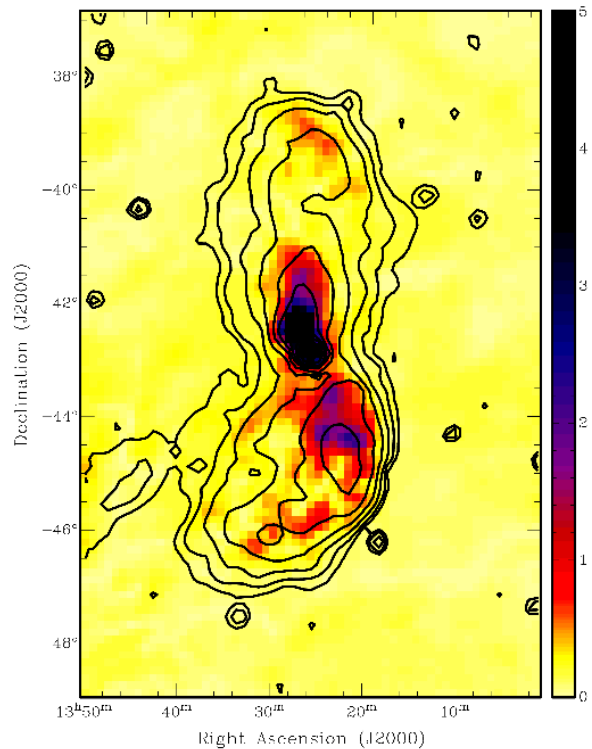


FIG. 1.— Polarized intensity (in Jy beam^{-1}) of the full observed region overlaid with the 1.4 GHz total intensity contours starting at $250 \text{ mJy beam}^{-1}$ and increasing by factors of two. Diffuse polarized emission is detected throughout the entire region due to the Galactic foreground. The degree of polarization of the strongly polarized regions ($p > 300 \text{ mJy beam}^{-1}$) within the lobes ranges from ~ 10 – 40% .

scope Compact Array (ATCA) at 1.4 GHz. They derived RMs for 281 background radio sources using essentially the same spectropolarimetric techniques as employed in this paper (see Section 2.3) with 24×8 MHz channels covering 1288 to 1480 MHz. In order to analyse the background radio sources without contamination from the large scale emission from Centaurus A, they filtered out the emission on large spatial scales by disregarding all visibilities from baselines shorter than 300 metres ($1.4 \text{ k}\lambda$). The high angular resolution ATCA observations ($\sim 40''$) thus provided an ensemble of background radio sources that were uncontaminated by any diffuse polarized emission and located along sight-lines both inside and outside the edge of the giant lobes.

2.3. Rotation Measure Analysis

Faraday rotation provides a direct diagnostic for the presence of magnetized thermal material though observations of the change in the state of polarization with wavelength as the radiation passes through magnetoionic media on its path to us. The Faraday depth (ϕ) of a particular region of polarized emission is defined as

$$\phi(L) = 0.81 \int_L^0 n_e B_{\parallel} dl \text{ rad m}^{-2}, \quad (1)$$

where n_e is the electron number density in cm^{-3} , B_{\parallel} is the line-of-sight magnetic field strength in μG and L is the distance through the magnetoionic region in parsecs. The total observed Faraday rotation measure (RM), de-

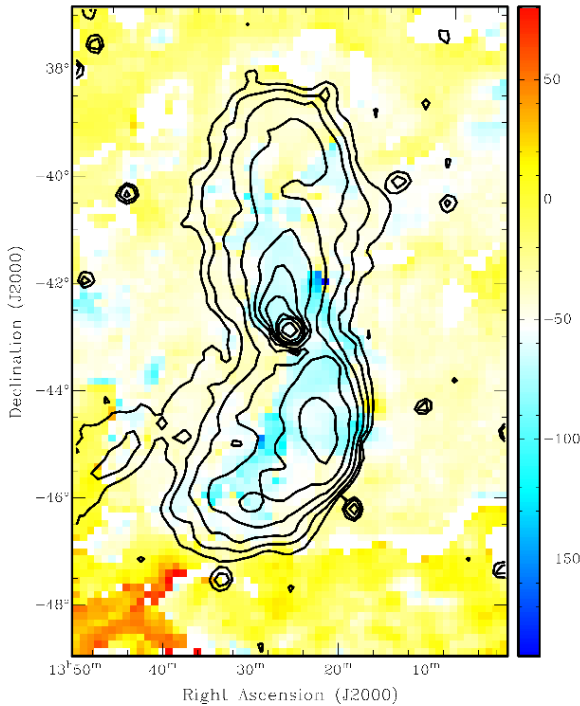


FIG. 2.— Faraday rotation measure (RM) derived at each $8' \times 8'$ pixel, overlaid with the 1.4 GHz total intensity contours. The range of RM on the color scale goes from -175 to $+100$ rad m^{-2} .

defined as $d\chi/d\lambda^2$, where χ is the polarisation angle, can have contributions from multiple regions along the line of sight. In the simplest case of a uniform external Faraday screen, the RM and Faraday depth are identical and the change in the polarization angle follows the relation

$$\chi = \chi_0 + \phi \lambda^2, \quad (2)$$

where χ_0 is the intrinsic ($\lambda = 0$) polarization angle.

To determine the RM we first constructed cubes of Stokes Q and U vs. λ^2 and applied the RM synthesis and RMCLEAN (Brentjens & de Bruyn 2005; Heald et al. 2009) techniques following the algorithm described by O'Sullivan et al. (2012). This generated a cube of polarized intensity ($p = \sqrt{Q^2 + U^2}$) at all Faraday depths from -3000 to $+3000$ rad m^{-2} from which the RM image was generated by extracting the RM at the peak polarized intensity. With the correct RM at each pixel the cube of polarized intensity is collapsed to form the polarized intensity image with the full sensitivity of the 168 MHz band.

Figure 1 shows the diffuse polarized emission detected from Centaurus A as well as from the Galaxy, which fills the entire field. The resolution in Faraday depth space ($\delta\phi$) of our experiment, defined by the FWHM of the Rotation Measure Spread Function (RMSF), is 310 rad m^{-2} . The largest magnitude Faraday depth we can reliably detect is ~ 3000 rad m^{-2} and the maximum detectable Faraday thickness is ~ 80 rad m^{-2} .

For a typical signal-to-noise ratio (S/N) of 50 to 100 on source, the error in the RM estimate at each pixel is $\sim 1\text{--}3$ rad m^{-2} ($\Delta RM \sim \delta\phi/(2 \times S/N)$). This error estimate relies on the assumption that there is only one dominant Faraday depth component within the FWHM of the RMSF; if there are multiple Faraday depth compo-

nents within our RMSF then we cannot uniquely specify their locations to better than 310 rad m^{-2} . However, for large S/N ratios the RMCLEAN algorithm may in principle be able to resolve components within the RMSF. We do not find any evidence for such components or for any significant broadening of the RMSF within the lobes of Centaurus A. In some regions of the observed field we find more than one peak in our Faraday depth spectrum. While the origin of these multiple Faraday depth components along the line of sight is interesting, none of these regions lie within the lobes of Centaurus A and are not included in our current study.

3. RESULTS & DISCUSSION

The measured RMs from the Parkes observations are shown in Figure 2 displaying a clear enhancement in the magnitude of the RM within the lobes of Centaurus A. Note that even with no Faraday rotating material in the vicinity of Centaurus A, we could observe such an enhancement in the magnitude of the observed RM in regions where the polarized emission from Centaurus A dominates over the Galactic emission. This can occur because the polarized emission of Centaurus A probes the full Faraday depth along the line of sight to us, while the diffuse Galactic polarized emission originates somewhere within our Galaxy and may only probe more local Faraday rotating regions depending on the exact location(s) of the polarized emission within our Galaxy. However, due to potential changes in the line of sight magnetic field direction, a longer line of sight does not necessarily mean a larger observed Faraday depth. The Galactic emission may also be subject to strong internal Faraday rotation effects resulting in a significantly lower RM than that measured from the polarized emission from Centaurus A.

3.1. Residual RM from Centaurus A

The mean RM of the background sources outside the lobes is -52.9 rad m^{-2} with a standard deviation of 29.2 rad m^{-2} (Feain et al. 2009). Therefore, the Faraday depth of our Galaxy is the dominant contributor to the total observed RM. The RMs from the 160 background sources located outside the lobes were used to remove the smooth part of the foreground Galactic Faraday rotating material. This was achieved by fitting a first-order two-dimensional polynomial to the point-source RMs outside the lobes. By subtracting this RM surface, with a gradient of ~ 6 $\text{rad m}^{-2} \text{ deg}^{-1}$, from both the background source RMs (inside and outside the lobes) and the RM of Centaurus A, we obtain the residual RM signal. The colored pixels in Figure 3 show the residual RM signal from the polarized emission of Centaurus A while the open circles show the residual RM from the background sources inside the lobes.

The mean of the magnitude of the residual RM from the polarized emission from Centaurus A greater than 300 mJy beam^{-1} is $\langle |RM| \rangle = 12.0 \pm 0.3$ rad m^{-2} (using the standard error of the mean)². The mean value of the RM from the Galactic polarized emission outside the lobes is approximately -27 rad m^{-2} with a standard

² Using only the same sightlines as the background sources we get $\langle |RM| \rangle = 13.0 \pm 1.9$ rad m^{-2} .

deviation of 23 rad m^{-2} while the mean polarized intensity is $\sim 52 \text{ mJy}$ with a standard deviation of 20 mJy . As the Galactic polarized emission becomes a significant fraction of the Centaurus A polarized emission towards the edges of the lobes, the systematic error in the measured RM will become large. Since we are unable to resolve the two contributions with our current dataset, we have only included in our analysis the regions within the lobes where the polarized emission from Centaurus A is strong enough to make the effect from the Galactic emission negligible (i.e., for Centaurus A polarized emission $\geq 300 \text{ mJy beam}^{-1}$, see Appendix).

It is possible that the residual RM signal could be explained by a degree-scale variation in the Galactic Faraday depth that happens to coincide with the orientation of the giant lobes and is not sampled by the background sources outside the lobes. We consider this unlikely but cannot definitively rule out such a scenario. There is a clear asymmetry in the distribution of signs of the residual RM between the Northern and Southern lobes. However, we are cautious not to over-interpret the sign of the residual RM since the smooth, foreground RM surface subtraction will not have removed any small angular-scale variations in the RM of our Galaxy. Therefore, residual RM contamination from our Galaxy may contribute to local enhancements in the residual RM magnitude as well as changes in the sign of the residual RM in patches throughout the lobes. Therefore, we defer a detailed analysis of individual features of RM amplitude and sign to a more detailed study of the polarisation properties of the giant lobes.

3.2. Origin of the Residual RM Signal

The observed residual RM signal may be due to Faraday rotation from thermal gas within the lobes, a thin boundary layer of swept up material surrounding the lobes or a large-scale fluctuation in the Galactic foreground Faraday depth coinciding with the position of the giant lobes. It is important to note that the subtraction using the fit to the background RMs just outside the lobes not only removes the smooth Faraday depth contribution of our Galaxy but also of any smooth RM component on large angular scales caused by the intra-group medium or an extended halo of magnetized thermal plasma surrounding the lobes.

The sign of the residual RM of the background sources within the lobes appears to correlate well with the RM from the diffuse emission (Figure 3). To quantitatively investigate the relation, we plot the residual background source RMs (RM_{bkg}) against the corresponding residual RMs of the polarized emission from Centaurus A ($\text{RM}_{\text{diffuse}}$) along the same sightline (Figure 4). There are some obvious discrepancies, which are not unexpected given the different scales probed by the ATCA ($\sim 50''$) and Parkes ($\sim 16'$) observations as well as the intrinsic scatter in the background source RMs (Feain et al. 2009). A correlation-coefficient of 0.54 between these two quantities shows that both the sign and amplitude of the two different RM measurements are related, with a best fit to the data giving $\text{RM}_{\text{bkg}} \sim 1.3\text{RM}_{\text{diffuse}}$.

Considering only the lines of sight in which the sign of RM_{bkg} and $\text{RM}_{\text{diffuse}}$ agree, we find a median ratio, $q \equiv \text{RM}_{\text{bkg}}/\text{RM}_{\text{diffuse}} \sim 1.5$. The median, rather than the mean, is quoted to avoid the results being skewed by

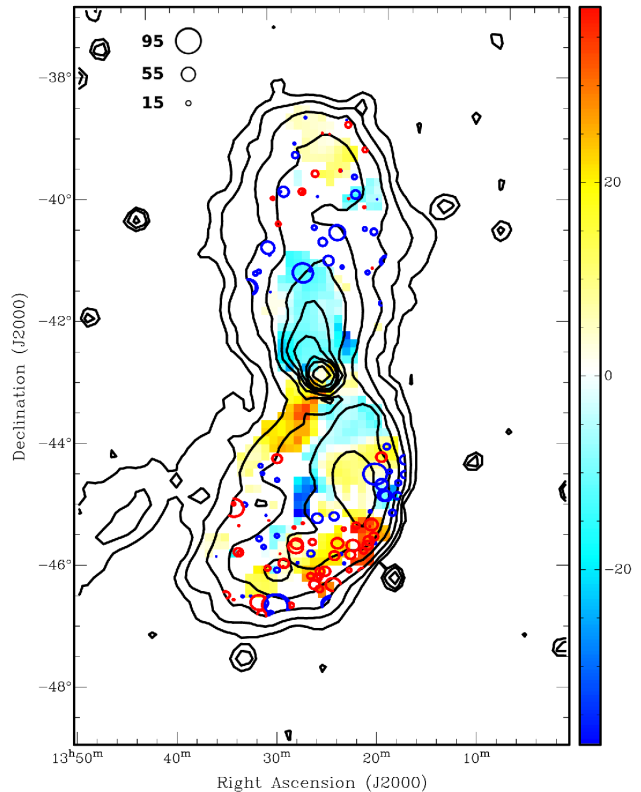


FIG. 3.— The residual RM (color scale ranging from -40 to $+40 \text{ rad m}^{-2}$) associated with Centaurus A after subtraction of the Faraday rotation due to foreground magnetoionic material. The residual RMs of the background sources inside the lobes are represented by circles whose size corresponds to the magnitude of the RM while red/blue circles indicate positive/negative signed RMs. The legend in the top left corner gives the magnitude of the RM, in rad m^{-2} , in relation to the size of the circles. There are no point source RMs towards the inner regions of the lobes because these regions were masked out due to imaging errors mainly caused by the bright core; see Feain et al. (2009) for details.

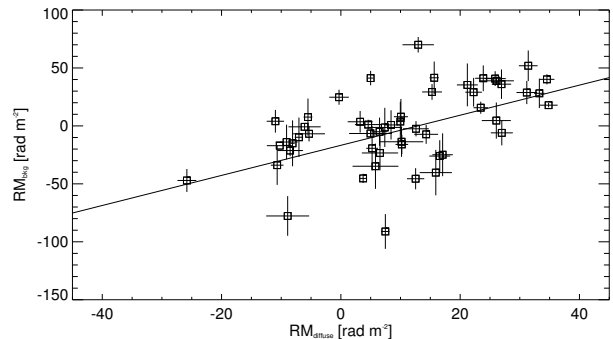


FIG. 4.— Plot of the background source residual RMs (RM_{bkg}) versus the residual RMs from the polarized emission of Centaurus A ($\text{RM}_{\text{diffuse}}$) at the same position, with both axes in rad m^{-2} . Solid line represents a best-fit line with slope 1.3 ± 0.1 .

a small number of outliers. Such a relation, with $q > 1$, is expected for most internal Faraday rotation models with $q = 2$ in the case of uniformly mixed emitting and rotating regions (e.g., Cioffi & Jones 1980). However, a value of $q \sim 2$ is also expected in the case of a thin boundary layer of magnetoionic material surrounding the

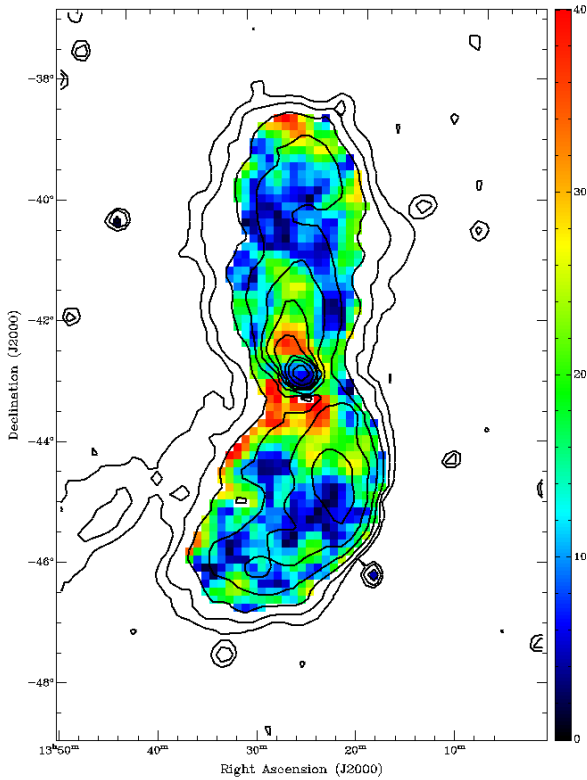


FIG. 5.— Fractional polarisation image ranging from 0–40% overlaid by the total intensity contours. A particularly interesting feature is the high fractional polarisation located $\sim 0.5^\circ$ South-West of the core. The fractional polarisation is not shown out to the edge of the total intensity contours because a dramatic increase that is unrelated to the physical properties of Centaurus A is observed. The effect is as a result of the steep falloff in total intensity while the Galactic polarized emission remains approximately constant.

lobes. This is assuming that the lobes and their immediate environments are symmetric in the sense that any postulated Faraday rotating region on the near side of the lobe is replicated on the far side. For the Northern lobe only, $q \sim 1.3$, while for the Southern lobe $q \sim 1.5$. This tentatively suggests that either a larger amount of gas is present within the Southern lobe or the lobe orientation is such that the Southern lobe is further away; however, it is difficult to claim this difference as significant given the smaller number of data points in the Northern lobe compared to the Southern lobe. Overall, the range $1.3 \leq q \leq 1.5$ supports an interpretation of internal Faraday rotation in which there is an asymmetric distribution of emitting and rotating regions within the lobes (e.g., Sokoloff et al. 1998), possibly with a small amount of Faraday rotation external to the lobes. However, we cannot discount entirely external effects due to the orientation of the lobes or residual RM contamination from the Galaxy (as described in Section 3.1). We avoid any in-depth modelling based on the value of q due to the sparse and unevenly sampled nature of the background sources. A much denser grid of background sources is required for more robust comparisons and detailed modelling of the distribution of emitting and rotating regions associated with the giant lobes.

Previous work by Feain et al. (2009) found a turbulent RM signal associated with the southern lobe due to either turbulent structure throughout the lobe or in a thin

skin surrounding the lobe boundary. If we assume that the residual large-scale RM signal we detect is due to a thin boundary layer of depth $\delta \sim 20$ kpc, then with an estimate of the line-of-sight magnetic field, B_{\parallel} , we can obtain the expected electron number density of the skin, $n_{e,skin}$. Based on the value of the magnetic field strength in the lobes of $B \sim 0.9 \mu\text{G}$, as derived in Abdo et al. (2010) based on broadband modelling of radio and γ -ray data, we can place a strong upper limit for the line-of-sight magnetic field in the skin of $B_{\parallel} \sim B/\sqrt{3} \sim 0.5 \mu\text{G}$. This leads to a conservative lower limit of $n_{e,skin} \sim 1.5 \times 10^{-3} (\text{RM}/12 \text{ rad m}^{-2})(B_{eq}/0.5 \mu\text{G})^{-1}(\delta/20 \text{ kpc})^{-1} \text{ cm}^{-3}$. This type of model is mainly based on the work of Bicknell et al. (1990) who used hydrodynamic simulations to show that Kelvin-Helmholtz instabilities may form on the surface of radio lobes and potentially cause advection of the lobe magnetic field into the surrounding medium.

The lobes of Centaurus A extend into a sparse group of galaxies (Karachentsev et al. 2007) with the Centaurus A host galaxy, NGC 5128 at the centre. An intergalactic medium (IGM) density of $n_{igm} \sim 10^{-3} \text{ cm}^{-3}$ was suggested by Bouchard et al. (2007) to explain a discontinuity in the HI properties of Centaurus A group dwarf galaxies through ram-pressure stripping arguments. However, this would seem excessively large for such a poor group of galaxies. In order to estimate a more plausible intragroup density at the extent (r) of the giant lobes, we use a standard profile $n_{igm}(r) \sim n_0(r/a_0)^{-b}$. This gives $n_{igm}(200 \text{ kpc}) \sim 10^{-4} \text{ cm}^{-3}$ for the typically derived values of $n_0 \sim 10^{-2} \text{ cm}^{-3}$, $a_0 \sim 10 \text{ kpc}$ and $b \sim 1.5$ (Mulchaey & Zabludoff 1998; Sun 2012), although the large scatter in the scaling parameters should be noted. The expansion of the lobes is expected to sweep up and possibly compress the intragroup medium around the edges of the lobes. Even if we consider a maximum compression factor of four, from a strong shock (which would be highly unlikely for the giant lobes), it is still not sufficient to reach $n_{e,skin} \sim 10^{-3} \text{ cm}^{-3}$. Furthermore, a rather low magnetisation of the IGM is expected on scales of hundreds of kiloparsecs from the group centre, certainly much less than the equipartition value in the lobes, unless some additional processes are able to substantially amplify the IGM magnetic field, as discussed in Bicknell et al. (1990) for example. Many theoretical models for the structure of extended lobes actually assume zero magnetisation of the ambient medium into which the lobes evolve (e.g., Gourgouliatos et al. 2010). Hence, the estimated value of $n_{e,skin} \sim 10^{-3} \text{ cm}^{-3}$ should be considered as a very conservative lower limit, corresponding to the maximum magnetisation of the IGM in the vicinity of the expanding lobes. Therefore, from the above arguments we conclude that the observed residual RM signal cannot be entirely explained by a thin skin scenario and that a significant fraction of thermal gas must be mixed throughout the lobe volume.

3.3. Depolarization of the Lobes

From the residual RM signal alone, we cannot determine exactly how much thermal material is likely to be mixed in with the relativistic lobe plasma. A potential discriminant comes from analysing the change in fractional polarisation with wavelength. For mixed radio-

emitting and Faraday-rotating regions, the polarization angle of radiation produced at different depths within the lobes is rotated by different amounts which leads to wavelength-dependent depolarisation (Burn 1966; Sokoloff et al. 1998). A thin-skin or boundary layer effectively acts as a foreground Faraday screen and does not depolarize the emission from the lobe (Bicknell et al. 1990). An unfortunate complication for the foreground screens is an effect known as external Faraday dispersion (Burn 1966; Tribble 1991). This occurs when many turbulent cells of magnetoionic material are within the telescope beam resulting in different amounts of Faraday rotation along different lines of sight which causes depolarisation when averaged across the beam area.

In order to better constrain the origin of the residual RM signal, we analysed the change in the degree of polarisation between 2.3, 1.4 and 0.96 GHz. The 2.3 GHz image was obtained from the S-band Polarization All Sky Survey (S-PASS), which recovers the absolute level of the polarized emission across the Southern sky (Carretti 2011) and hence provides a very robust estimate for the level of polarized emission from Centaurus A at 2.3 GHz. The 0.96 GHz fractional polarisation image was created using the Stokes I and p contour plots from Cooper et al. (1965). Digital copies of these images are not available so we used the algorithm of Westphalen (1995) to reliably represent the contour plots in digital form. Given that the noise is not recovered in the digitized images, we limit our analysis to the highest signal-to-noise (S/N) areas where the estimated error is $\lesssim 10\%$ (Westphalen 1995). Both the 2.3 and 1.4 GHz images were smoothed, in Q and U to the resolution of the 0.96 GHz image.

3.4. External Depolarisation Model

For our depolarisation analysis we have chosen four positions which have high S/N as well as small observed variation in RM across the beam so that the depolarising effects of external Faraday dispersion are minimized. To model the depolarising effect of a foreground screen with

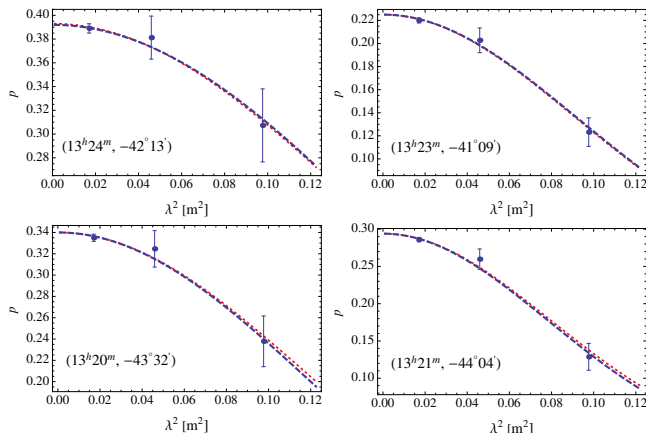


FIG. 6.— Plots of the degree of polarisation (p) versus wavelength squared (λ^2) for four regions of the giant lobes of Centaurus A at 2.3, 1.4 and 0.96 GHz. We chose areas with high S/N in p as well as small variations in RM across an area equivalent to the 0.96 GHz beamsize. The dotted (red) curves represent a model of depolarisation solely from external Faraday dispersion while the dashed (blue) curves represent a model combining both internal Faraday rotation and external Faraday dispersion. In the top right and top left plots, the dashed (blue) and dotted (red) curves are almost identical.

a Gaussian random magnetic field we use

$$p = p_0 \exp(-2\sigma_{\text{RM}}^2 \lambda^4), \quad (3)$$

where p_0 is the intrinsic degree of polarized emission from the lobes and σ_{RM} describes the RM fluctuations on scales smaller than the observing beam.

Figure 6 shows the fractional polarisation versus wavelength squared for two positions in the Northern lobe, ($13^{\text{h}}27^{\text{m}}, -42^{\circ}29'$) and ($13^{\text{h}}26^{\text{m}}, -41^{\circ}25'$), and two in the Southern lobe, ($13^{\text{h}}23^{\text{m}}, -43^{\circ}49'$) and ($13^{\text{h}}24^{\text{m}}, -44^{\circ}21'$). For the chosen positions, the variation in RM across an area the size of the 0.96 GHz beam is less than the estimated error of the individual RM measurements. The dotted (red) curves in Figure 6 represent a fit to the data using equation 3 with values of σ_{RM} ranging from 3.5–6.3 rad m^{-2} . Table 1 lists the values of the fitted parameters with their respective error estimates. From this we see that depolarisation from an external Faraday screen can, in principle, explain the total depolarisation observed at these four positions of the giant lobes. However, we note that fluctuations in the complex polarisation can become dominant at long wavelengths resulting in a much weaker than expected decrease in the degree of polarisation due to external Faraday dispersion (Tribble 1991; Sokoloff et al. 1998). Hence, for Centaurus A, the observed depolarisation may not be very well described by an exponential decrease in the degree of polarisation.

In Figure 1 we can see a strong asymmetry between the polarized intensity in the inner parts of the Northern and Southern giant lobes, the origin of which could be attributed to the Laing-Garrington effect (Laing 1988; Garrington et al. 1988). This effect is commonly assigned to a halo of thermal gas, threaded by a turbulent magnetic field, surrounding the radio galaxy (Garrington & Conway 1991). In this case, the depolarisation is larger for the assumed more distant Southern lobe, in which the path length through the surrounding gas is larger. However, there is no compelling evidence for the exact orientation of the lobes. The effect may also be explained by internal differences between the two lobes and/or from a gradient, with Galactic latitude, in the properties of the foreground Galactic Faraday screen.

In order to comment further on this issue, we show the fractional polarisation within the giant lobes in Figure 5. One of the most interesting features of this image is the high degree of polarisation located $\sim 0.5^{\circ}$ South-West of the bright core. We speculate that this region may be the oppositely-directed counterpart of the well studied Northern middle lobe (Morganti et al. 1999), which until now had no observed Southern counterpart. This “Southern middle lobe” may have lost its structure and merged with the outer/older radio lobe after uplifting and mixing with a large amount of gas from the host galaxy. This scenario would require some asymmetry in the distribution of gas within the host galaxy which is not unreasonable in the aftermath of a merger event (Sparke 1996).

In fact, a recent study by Bell & Comeau (2012) found, for sources exhibiting the Laing-Garrington effect, that the jet brightness asymmetry on kpc-scales cannot be explained by beaming and therefore must be intrinsic (in cases where the estimated kpc-scale outflow speeds are close to $0.1c$). They conclude that a Laing-Garrington

TABLE 1
EXTERNAL FARADAY DISPERSION MODEL
PARAMETERS.

Position	p_0 (%)	σ_{RM} (rad m ⁻²)
(13 ^h 27 ^m , -42°29')	39.3 ± 0.4	3.5 ± 0.3
(13 ^h 26 ^m , -41°25')	22.5 ± 0.2	5.5 ± 0.3
(13 ^h 23 ^m , -43°49')	34.0 ± 0.5	4.2 ± 0.4
(13 ^h 24 ^m , -44°21')	29.4 ± 0.6	6.3 ± 0.5

NOTE. — Col. 1: Position of extracted data in RA and Dec in J2000. Col. 2: intrinsic degree of polarisation. Col. 3: variation in the external RM on scales smaller than the beam.

TABLE 2
INTERNAL FARADAY ROTATION MODEL PARAMETERS.

Position	$ \phi $ (%)	σ_ϕ (rad m ⁻²)	σ_{RM} (rad m ⁻²)
(13 ^h 27 ^m , -42°29')	10.2 ± 1.7	1.7 ± 0.7	1.2 ± 0.6
(13 ^h 26 ^m , -41°25')	10.0 ± 0.7	3.0 ± 0.2	4.1 ± 0.3
(13 ^h 23 ^m , -43°49')	10.1 ± 1.2	2.1 ± 0.4	2.7 ± 0.4
(13 ^h 24 ^m , -44°21')	10.1 ± 0.9	2.1 ± 0.6	5.5 ± 0.4

NOTE. — Col. 1: Position of extracted data in RA and Dec in J2000. Col. 2: internal Faraday depth of the lobes. Col. 3: internal Faraday dispersion within the lobes. Col. 3: variation in the external RM on scales smaller than the beam.

effect due to intrinsic differences in the Faraday rotating material within radio galaxy lobes cannot be discounted. Based on these results and our arguments in Section 3.2 for a significant fraction of thermal material mixed in with the relativistic plasma of the lobes, we next consider a model in which a significant fraction of the observed depolarisation (and residual RM signal) is due to internal Faraday rotation.

3.5. Internal Depolarisation Model

If the observed Faraday rotation and depolarisation are due to thermal gas within the lobes, we can estimate the number density of the gas using an internal Faraday rotation model that accounts for depolarisation from the ordered magnetic field (B_{ord}) as well as from the random magnetic field (B_{rdm}) within the lobes. In this model, we consider the simplest case of a Gaussian distribution of Faraday depths with mean ϕ and standard deviation σ_ϕ in a slab with a linear depth L along the line of sight (Burn 1966; Sokoloff et al. 1998). The intrinsic ($\lambda = 0$) fraction of polarized emission from Centaurus A (p_0) is then modified following

$$p = p_0 \left(\frac{1 - e^{-2\sigma_\phi^2 \lambda^4 + 2i\lambda^2 \phi}}{2\sigma_\phi^2 \lambda^4 - 2i\lambda^2 \phi} \right) e^{-2\sigma_{\text{RM}}^2 \lambda^4}, \quad (4)$$

where $\sigma_\phi = 0.81n_e B_{\text{rdm}} (Ld)^{1/2}$ with d representing the scale of magnetic field fluctuations of the random magnetic field (B_{rdm}) such that the number of cells along the line of sight is L/d . We have also included the effect of external Faraday dispersion, as described in Section 3.4, and use the same values of p_0 .

The dashed (blue) curves in Figure 6 represent fits to the data using the above model for each of the four lobe positions. In all cases, we find the magnitude of the in-

ternal Faraday depth, $|\phi| \sim 10$ rad m⁻² with σ_ϕ ranging from 1.7 to 3.0 rad m⁻² and σ_{RM} ranging from 1.2 to 5.5 rad m⁻². Since we have only three data points and have to fit for three variables, this essentially guarantees a good fit, perhaps giving false confidence in the appropriateness of the model. Hence, we consider the fitted parameters of this model, shown in Table 2, as reasonable estimates of the model parameters which can describe the observed depolarisation given our current observational knowledge.

Due to the random component of the magnetic field in the lobes, we expect to see an excess dispersion in the RM within the lobes over the RM dispersion outside the lobes (i.e., σ_ϕ). However, this is difficult to disentangle from the turbulent magnetoionic medium of our Galaxy that likely varies throughout the entire field as well as from effects more local to the source due to the orientation of the lobes (e.g. the Laing-Garrington effect). The standard deviation of the RM from the diffuse Galactic emission (outside the lobes) is ~ 12 rad m⁻² while the RM of the polarized emission from Centaurus A has a standard deviation of ~ 14 rad m⁻². This difference cannot be regarded as significant, given our individual measurement errors (Section 2.3), but it is not inconsistent with the fitted values of σ_ϕ used to describe the depolarisation in the lobes.

The total magnetic field strength (B_{tot}) in the Northern and Southern lobes has been estimated at ~ 0.9 μG from the modelling of radio and γ -ray data (Abdo et al. 2010). The intrinsic degree of polarization of synchrotron radiation (p_i) is reduced from its maximum level according to the relation $p_0 = p_i B_{\text{ord}}^2 / B_{\text{tot}}^2$ where $B_{\text{tot}}^2 = B_{\text{ord}}^2 + B_{\text{rdm}}^2$ and $p_i = (3 - 3\alpha)/(5 - 3\alpha)$, with α representing the spectral index (Burn 1966). Therefore, using the spectral index of particular regions of the giant lobes obtained from Hardcastle et al. (2009) and the mean observed fractional polarization from our observations, we can estimate the strength of the ordered (B_{ord}) and random (B_{rdm}) magnetic field components. For example, at the position (13^h23^m, -41°09') we have $p_0 = 22.5\%$, therefore $B_{\text{ord}} \sim B_{\text{rdm}} \sim B_{\parallel} \sim 0.5$ μG . Considering a path length through the lobes of $L \sim 200$ kpc and a magnetic field fluctuation scale of $d \sim 20$ kpc, we use $\sigma_\phi = (5 \times 10^4)n_e B_{\text{rdm}}$ and $\phi \sim (2.5 \times 10^5)n_e B_{\parallel}$ to find, for the four selected regions of the lobes, $n_e \sim (0.9 - 1.3) \times 10^{-4}$ cm⁻³.

Feain et al. (2009) provided an upper limit on the volume-averaged thermal electron density of the lobes of $\langle n_e \rangle \lesssim 1.3 \times 10^{-4} (0.5/B_{\parallel})^{-1}$ cm⁻³, where in this case we use $B_{\parallel} \sim 0.5$ μG instead of the equipartition value of 1.3 μG used in their paper. This limit was based on sampling of the background sources inside the lobes, probing a distribution presumably more inhomogeneous than the sparse sampling of the background sources could detect. However, the limit is not inconsistent with our results. Our measured value of $n_e \sim 10^{-4}$ cm⁻³ based on our internal Faraday rotation interpretation provides a very good description of all the current observables (i.e., the residual RM signal, the depolarisation and the excess RM dispersion associated with the lobes). Although we cannot definitively rule out external Faraday effects as an explanation for the total amount of observed depolarisation, we prefer the internal Faraday rotation inter-

pretation since it better explains all the observational evidence. Taking this as our preferred model we now investigate some of the important consequences for the giant lobes.

3.5.1. Implications for the Giant Lobes

In order to calculate the pressure in the lobes due to the thermal gas ($p_{th} \sim n_e kT$), we require an estimate for the temperature (T) of the gas. Recent X-ray results from a small region of the southern lobe found an excess of diffuse, thermal emission from Centaurus A over the background, with a best-fit gas temperature of $kT \sim 0.5$ keV and a number density of $\sim 10^{-4} \text{ cm}^{-3}$ (Stawarz et al. 2012), in excellent agreement with the density estimate made in Section 3.3 above. Interestingly, this leads to a thermal pressure, $p_{th} \sim 8 \times 10^{-14} \text{ erg cm}^{-3}$ which is approximately equal to the total non-thermal pressure, $(p_{e\pm} + U_B) \sim 8 \times 10^{-14} \text{ erg cm}^{-3}$ (Abdo et al. 2010; Stawarz et al. 2012), where the magnetic energy density $U_B \equiv B_{tot}^2/8\pi$. It is important to note that our derivations do not depend on an equipartition assumption, and therefore, on the unknown contribution of relativistic protons. They depend instead on the magnetic field value derived from the broadband modelling in Abdo et al. (2010), whose primary assumption is that the detected γ -ray flux is solely due to the inverse-Compton emission of the radio emitting electrons. The derived magnetic field value is thus consistent with the case of an approximate energy equipartition between the magnetic field, radiating electrons, and potentially any relativistic protons present (i.e. $U_B \sim U_e \gtrsim U_p$).

The majority of extended lobes in low-power radio galaxies are found to be under-pressured or in approximate pressure equilibrium with their external environment, under the assumption of energy equipartition between the magnetic field and radio-emitting electrons within the lobes (Morganti et al. 1988; Croston et al. 2008). Hence, those lobes must be either far from the magnetic field–relativistic electrons energy equipartition, or there must be additional pressure provided by particles contributing only weakly to the observed non-thermal continuum of the lobes to maintain the structure of the expanding cavity. Here we have found direct evidence for thermal particles contributing substantially to the internal pressure in the giant lobes of Centaurus A. Even so, approximate equipartition between the thermal and non-thermal gas pressures still cannot entirely explain the pressure mis-match in all low-power radio galaxies, indicating that relativistic protons may have a substantial contribution in some cases.

Based on the derived number density of $\sim 10^{-4} \text{ cm}^{-3}$ and the estimated volume $V \sim 2 \times 10^{71} \text{ cm}^3$ (Hardcastle et al. 2009; Abdo et al. 2010), we find that the total mass of the thermal gas within the lobes is $M_{th} \sim n_{th} m_H f_V V \sim 2 \times 10^{10} M_\odot$, where m_H is the mass of ionized hydrogen and we use a volume filling factor $f_V \sim 1$. Similar amounts of gas inferred from metal-enriched outflows have also been observed in a number of other radio galaxies (Simionescu et al. 2009; Kirkpatrick et al. 2009; McNamara & Nulsen 2012). We consider the possibility that the vast majority of the thermal material has either been entrained as the jet ploughed through the interstellar medium (ISM) of the host galaxy (Laing & Bridle 2002) and/or pushed out by the over-pressured

lobes as they expand outwards (Begelman & Cioffi 1989; Churazov et al. 2001). Entrainment of thermal material is considered as the most likely mechanism for decelerating relativistic jets (Bicknell 1994) but the amount of material required is of the order of $10^{-3} M_\odot/\text{yr}$ (Laing & Bridle 2002). Therefore, this is highly unlikely to be able to provide the necessary $200 M_\odot/\text{yr}$ required by our results, for a lobe age of the order of 100 Myr (Hardcastle et al. 2009). More likely is that the expanding lobes push out large amounts of gas from the host galaxy atmosphere/halo through successive episodes of jet activity. In Centaurus A there is evidence for at least four episodes of activity: the giant outer lobes, the Northern middle lobe (Morganti et al. 1999), the inner lobes (Burns et al. 1983), and the parsec-scale jets (Tingay et al. 2001).

Recent simulations (Wagner & Bicknell 2011) have shown the importance of inhomogeneity of the ISM which can cause deflection of the jet flow, allowing the radio source to effect a much larger volume of the host galaxy. In this way, a large amount of gas can be swept up by the influence of the jet at large distances from the center of the galaxy, possibly explaining the substantial amount of gas we have detected within the lobes. Such a large removal of gas from the host galaxy provides a direct mechanism for suppressing star formation while also limiting the amount of gas that can cool and fall back towards the center of the galaxy, which may also limit the growth of the central supermassive black hole. It is also possible that a significant fraction of the mass of thermal gas within the lobes was entrained from the intergroup medium and dispersed over the entire lobe volume. More detailed simulations with synthetic Faraday rotation observations will be required to help distinguish between these scenarios.

4. CONCLUSIONS

We have presented results from a spectropolarimetric study, using the Parkes radio telescope at 1.4 GHz, investigating the Faraday rotation of the diffuse polarized emission from the giant lobes of the radio galaxy, Centaurus A. Using previous results from an RM grid of background radio sources just outside the lobes (Feain et al. 2009), the smooth foreground contribution to the observed RM from Centaurus A was subtracted, leaving a mean residual RM signal of $\sim 12 \text{ rad m}^{-2}$.

Investigation of whether the residual RM signal comes from a thin-skin/boundary layer of magnetoionic material surrounding the lobes or from thermal gas internal to the lobes, found the thin-skin scenario highly unlikely given that it requires at least an order of magnitude enhancement of the swept up gas over the expected intra-group density on these scales. It should be noted that we cannot conclusively rule out that the residual RM signal comes from a degree-scale fluctuation in the smooth Galactic foreground that was not sampled by the ensemble of background sources outside the lobes and happens to align with the orientation of the giant lobes.

From our investigation of the degree of polarisation at three separate frequencies (2.3, 1.4 & 0.96 GHz) at four positions of high S/N, we find strong depolarisation which cannot be explained solely by the effects of beam depolarisation. Considering all the available data, we consider depolarisation due to Faraday rotation within

the lobes as our preferred scenario, even in the presence of external Faraday dispersion from a foreground screen. In this case, we estimate the number density of the thermal gas $n_e \sim 10^{-4} \text{ cm}^{-3}$ which gives a total ionized gas mass within the lobes of $\sim 10^{10} M_\odot$. Recent X-ray observations of a small region of the southern lobe also find evidence for thermal gas within the lobe with a temperature of $\sim 0.5 \text{ keV}$ (Stawarz et al. 2012). From this we estimate that the thermal pressure within the lobes is approximately equal to the non-thermal pressure implying that the thermal gas, radio-emitting electrons and magnetic field are all in approximate equipartition with each other.

Future radio polarisation observations are required to have much wider λ^2 -coverage to provide the high resolution in Faraday depth space needed to uniquely separate the internal and external Faraday rotating components. Indeed the planned Global Magneto-Ionic Medium Survey (GMIMS) which covers 300–1800 MHz (Wolleben et al. 2009) provides an excellent opportunity to resolve

the Faraday rotation structure in the giant lobes of Centaurus A.

ACKNOWLEDGEMENTS

The Parkes radio telescope and Australia Telescope Compact Array are funded by the Commonwealth of Australia for operation as a National Facility managed by CSIRO. B.M.G. acknowledges the support of the Australian Research Council through grant FL100100114. The authors would like to thank Marijke Haverkorn for her help with the observations, as well as Shea Brown, Alex Hill and Leith Godfrey for helpful comments and discussions. We also thank the referee for providing several important comments which helped improve this paper. The National Radio Astronomy Observatory is a facility of the National Science Foundation operated under cooperative agreement by Associated Universities, Inc.

Facilities: Parkes ATCA

REFERENCES

- Abdo, A. A., Ackermann, M., Ajello, M., et al. 2010, *Science*, 328, 725
- Aguirre, A., Hernquist, L., Schaye, J., et al. 2001, *ApJ*, 561, 521
- Begelman, M. C., Blandford, R. D., & Rees, M. J. 1984, *Reviews of Modern Physics*, 56, 255
- Begelman, M. C., & Cioffi, D. F. 1989, *ApJL*, 345, L21
- Bell, M., & Comeau, S. 2012, arXiv preprint arXiv:1211.5337
- Best, P. N., Kaiser, C. R., Heckman, T. M., & Kauffmann, G. 2006, *MNRAS*, 368, L67
- Bicknell, G. V. 1994, *Australian Journal of Physics*, 47, 669
- Bicknell, G. V., Cameron, R. A., & Gingold, R. A. 1990, *ApJ*, 357, 373
- Birzan, L., McNamara, B. R., Nulsen, P. E. J., Carilli, C. L., & Wise, M. W. 2008, *ApJ*, 686, 859
- Bouchard, A., Jerjen, H., Da Costa, G. S., & Ott, J. 2007, *AJ*, 133, 261
- Bower, R. G., Benson, A. J., Malbon, R., et al. 2006, *MNRAS*, 370, 645
- Brentjens, M. A., & de Bruyn, A. G. 2005, *A&A*, 441, 1217
- Burn, B. J. 1966, *MNRAS*, 133, 67
- Burns, J. O., Feigelson, E. D., & Schreier, E. J. 1983, *ApJ*, 273, 128
- Carretti, E. 2011, *Journal of Astrophysics and Astronomy*, 32, 457
- Churazov, E., Brüggen, M., Kaiser, C. R., Böhringer, H., & Forman, W. 2001, *ApJ*, 554, 261
- Cioffi, D. F., & Jones, T. W. 1980, *AJ*, 85, 368
- Cooper, B. F. C., Price, R. M., & Cole, D. J. 1965, *Australian Journal of Physics*, 18, 589
- Croston, J. H., Hardcastle, M. J., Birkinshaw, M., Worrall, D. M., & Laing, R. A. 2008, *MNRAS*, 386, 1709
- Croton, D. J., Springel, V., White, S. D. M., et al. 2006, *MNRAS*, 365, 11
- Dunn, R. J. H., Fabian, A. C., & Taylor, G. B. 2005, *MNRAS*, 364, 1343
- Emerson, D. T., & Graeve, R. 1988, *A&A*, 190, 353
- Farnsworth, D., Rudnick, L., & Brown, S. 2011, *AJ*, 141, 191
- Feain, I. J., Ekers, R. D., Murphy, T., et al. 2009, *ApJ*, 707, 114
- Feain, I. J., Cornwell, T. J., Ekers, R. D., et al. 2011, *ApJ*, 740, 17
- Furlanetto, S. R., & Loeb, A. 2001, *ApJ*, 556, 619
- Garrington, S., Leahy, J., Conway, R., & Laing, R. 1988, *Nature*, 331, 147
- Garrington, S. T., & Conway, R. G. 1991, *MNRAS*, 250, 198
- Gourgouliatos, K. N., Braithwaite, J., & Lyutikov, M. 2010, *MNRAS*, 409, 1660
- Hardcastle, M. J., Cheung, C. C., Feain, I. J., & Stawarz, L. 2009, *MNRAS*, 393, 1041
- Harris, G. L. H., Rejkuba, M., & Harris, W. E. 2010, *PASA*, 27, 457
- Heald, G., Braun, R., & Edmonds, R. 2009, *A&A*, 503, 409
- Karachentsev, I. D., Tully, R. B., Dolphin, A., et al. 2007, *AJ*, 133, 504
- Kirkpatrick, C. C., Gitti, M., Cavagnolo, K. W., et al. 2009, *ApJL*, 707, L69
- Kronberg, P. P., Colgate, S. A., Li, H., & Dufton, Q. W. 2004, *ApJL*, 604, L77
- Laing, R. 1988, *Nature*, 331, 149
- Laing, R. A., & Bridle, A. H. 1987, *MNRAS*, 228, 557
- . 2002, *MNRAS*, 336, 1161
- Law, C. J., Gaensler, B. M., Bower, G. C., et al. 2011, *ApJ*, 728, 57
- Mao, S. A., McClure-Griffiths, N. M., Gaensler, B. M., et al. 2012, *ApJ*, 759, 25
- McNamara, B. R., Kazemzadeh, F., Rafferty, D. A., et al. 2009, *ApJ*, 698, 594
- McNamara, B. R., & Nulsen, P. E. J. 2012, *New Journal of Physics*, 14, 055023
- Morganti, R., Fanti, R., Gioia, I. M., et al. 1988, *A&A*, 189, 11
- Morganti, R., Killeen, N. E. B., Ekers, R. D., & Oosterloo, T. A. 1999, *MNRAS*, 307, 750
- Mulchaey, J. S., & Zabludoff, A. I. 1998, *ApJ*, 496, 73
- O’Sullivan, S. P., Brown, S., Robishaw, T., et al. 2012, *MNRAS*, 421, 3300
- Perley, R. A., Bridle, A. H., & Willis, A. G. 1984, *ApJS*, 54, 291
- Reuland, M., van Breugel, W., de Vries, W., et al. 2007, *AJ*, 133, 2607
- Reynolds, J. E. 1994, *ATNF Technical Memo Series*, 39.3/040
- Simionescu, A., Werner, N., Böhringer, H., et al. 2009, *A&A*, 493, 409
- Sokoloff, D. D., Bykov, A. A., Shukurov, A., et al. 1998, *MNRAS*, 299, 189
- Spangler, S. R., & Sakurai, T. 1985, *ApJ*, 297, 84
- Sparke, L. S. 1996, *ApJ*, 473, 810
- Stawarz, L., Tanaka, Y. T., Madejski, G., et al. 2012, *ApJ*, submitted, arXiv:1210.4237
- Sun, M. 2012, *New Journal of Physics*, 14, 045004
- Tingay, S. J., Preston, R. A., & Jauncey, D. L. 2001, *AJ*, 122, 1697
- Tribble, P. C. 1991, *MNRAS*, 250, 726
- Wagner, A. Y., & Bicknell, G. V. 2011, *ApJ*, 728, 29
- Westphalen, G. 1995, in *Astronomische Gesellschaft Abstract Series*, Vol. 11, *Astronomische Gesellschaft Abstract Series*, ed. G. Klare, 246
- Wolleben, M., Landecker, T. L., Carretti, E., et al. 2009, in *IAU Symposium*, Vol. 259, *IAU Symposium*, 89–90

APPENDIX

For observations which have more than one source of polarized emission along the line of sight with different Faraday depths and/or Faraday thicknesses, the measured RM can vary with wavelength (Law et al. 2011; Farnsworth et al. 2011; O’Sullivan et al. 2012). Since we detect both the diffuse polarized emission from our Galaxy as well as the polarized emission from Centaurus A, we need to consider how this may affect our measured RM. The RM resolution of 310 rad m^{-2} limits our ability to distinguish between multiple regions of polarized emission whose Faraday depth differs by less than this amount. Therefore, we use models of two line-of-sight polarized components with different Faraday depths to investigate at what points within the lobes of Centaurus A our measured RMs accurately represent the true Faraday depth of the polarized emission from Centaurus A.

To illustrate the effect, we define a two component model

$$P = p_0 \left(\frac{1 - e^{-2\sigma_\phi^2 \lambda^4 + 2i\lambda^2 \phi}}{2\sigma_\phi^2 \lambda^4 - 2i\lambda^2 \phi} \right) e^{2i(\chi_0 + \phi_g \lambda^2)} e^{-2\sigma_{\text{RM}}^2 \lambda^4} + p_g \left(\frac{\sin \phi_g \lambda^2}{\phi_g \lambda^2} e^{2i(\chi_{0g} + \frac{1}{2}\phi_g \lambda^2)} \right) e^{-2\sigma_{\text{RM}}^2 \lambda^4}, \quad (5)$$

in which the polarized emission of our Galaxy (p_g) is described by a uniform slab (Burn 1966) of Faraday depth ϕ_g while the Centaurus A model is described in Section 3.5. We use the values for position ($13^{\text{h}}27^{\text{m}}, -42^\circ29'$) listed in Table 2 with the Galactic Faraday depth, $\phi_g = -58 \text{ rad m}^{-2}$ taken from the fit for the foreground RM surface. The intrinsic polarization angle of the Centaurus A emission, $\chi_0 = 30^\circ$, is taken from a derotated $\lambda = 0$ polarization angle at this position. For the Galactic emission, we use a completely arbitrary value of $\chi_{0g} = 90^\circ$. We then set $p_0 = 1.0$ and plot the results for various fractions of p_g/p_0 , shown in Figure 7.

The top panel of Figure 7 shows the Faraday rotation measure calculated as $\text{RM} = d\chi/d\lambda^2$, where $\chi = \frac{1}{2} \arctan U/Q$ and $P = Q + iU$. This shows that as long as $p_g/p_0 \leq 0.15$ the possible systematic error in the measured RM is less than 3 rad m^{-2} , where the expected RM is $\frac{1}{2}\phi + \phi_g$ (solid horizontal line). As the Galactic polarized emission (mean value $\sim 52 \text{ mJy}$) becomes a larger fraction of the Centaurus A polarized emission, the systematic error in the measured RM becomes much larger (dotted line). Since we are unable to disentangle the two contributions with our current dataset, we have only included in our calculations the regions within the lobes of Centaurus A where the polarized emission is $\gtrsim 300 \text{ mJy beam}^{-1}$. This value roughly corresponds to $p_g/p_0 \lesssim 0.15$, which means that even in the regions of lowest polarized intensity the potential systematic error in the RM is less the mean measurement error within the lobes of $\sim 3 \text{ rad m}^{-2}$.

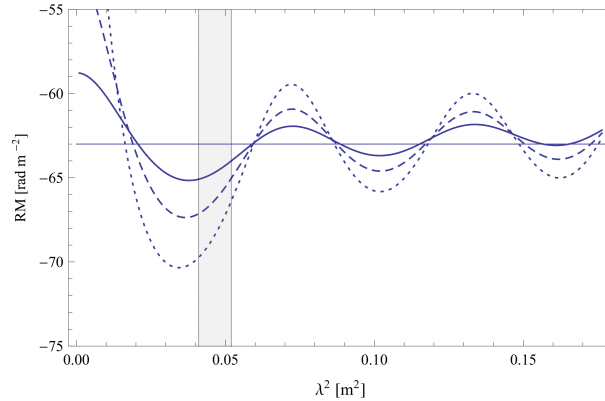


FIG. 7.— Plot of RM vs. λ^2 , to illustrate the RM variation due to sampling multiple regions of mixed polarized emission and Faraday rotation along a single line of sight. The RM is calculated as $d\chi/d\lambda^2$ and the solid horizontal line is the expected RM (see Appendix for details). Solid line: $p_g/p_c = 0.15$, dashed line: $p_g/p_c = 0.3$, dotted line: $p_g/p_c = 0.5$. The shaded areas indicate the range of λ^2 space covered by our observations.